J. Condensed Matter Nucl. Sci. 23 (2017) 1–26

Research Article

# A Study on the Possibility of Initiating Tungsten Alpha Decay Using Electric Explosion

L.I. Urutskoev*

*The Russian Presidential Academy of National Economy and Public Administration (RANEPA), 82/5 Prospect Vernadskogo, Moscow 119571, Russian Federation*

D.V. Filippov

*Russian Foreign Trade Academy of the Ministry for Economic Development of the Russian Federation (RFTA), 4A Pudovkina Str., Moscow 119285, Russia*

A.O. Birykov

*Presidential Executive Office*

G.I. Astapenko, D.A. Voitenko and A.A. Markoliya

*Sukhumi Institute of Physics and Technology, Sukhumi, Republic of Abkhazia, 665 Kodori Highway, Sukhumi, Republic of Abkhazia*

K.A. Alabin

*Prokhorov General Physics Institute, Russian Academy of Sciences, Vavilov Str. 38, 119991 Moscow, Russia*

**Abstract**

Experiments with electric explosion of tungsten wires are described. These are intended to check the results of G.L. Wendt and C.E. Irion's experiments published in 1922. The historical and theoretical background of this study are described in detail. The gas phase formed in the chamber after the electric explosion was carefully studied in the experiments. The results of the study do not contradict with the results of the Wendt and Irion experiments.
© 2017 ISCMNS. All rights reserved. ISSN 2227-3123

*Keywords:* Alpha- beta-decay, Alpha-decay, Electrical explosion of conductors, Gas phase analysis, Gas mass-spectrometer, Optical spectral line

*Corresponding author. E-mail: urleon@yandex.ru

© 2017 ISCMNS. All rights reserved. ISSN 2227-3123

## 1. Historical Background, Experiment of G.L. Wendt and C.E. Irion [1]

In the second decade of the last century, work on the use of electric explosion of conductors (EEC) for laboratory simulation of astrophysical processes were started in the United States. The pioneer of this new research field was John August Anderson, who demonstrated that by using a high-current EEC one can reach very high temperatures [2]. The temperature of the plasma, which was generated by electric explosion of wire, was $T \approx 2 \times 10^4$ K as estimated by Anderson using the luminance method [2]. It was the highest recorded temperature obtained under laboratory conditions up to that time. Staff at the Chicago University chemical laboratory, Gerald Wendt and Clarence Irion, decided to use the electric explosion method developed by J. Anderson to test a hypothesis. Their hypothesis was based on two facts firmly established by then: the temperature of the sun surface is about $6 \times 10^3$ K and there are no characteristic optical lines of heavy chemical elements in the visible spectrum.

Based on these facts, Wendt and Irion suggested that the absence of the spectral lines of heavy chemical elements in the radiation spectrum of the sun and other stars can be explained by the fact that heavy chemical elements are unstable at solar temperatures.

In 1919, E. Rutherford, using high energy $\alpha$-particles, was able to produce a nuclear reaction of $^{14}$N nuclei. Thus, the fundamental possibility of nuclear reactions in laboratory conditions was demonstrated. However, in the early 1920s, the difference in scale of energies of atomic and nuclear phenomena was not yet been fully understood. Probably, therefore, the emergence of the Irion and Wendt hypothesis did not trigger strong rejection in the scientific community, as it would have if such a hypothesis had been proposed 5 or 10 years later.

The idea of the experiment of Wendt and Irion was to pass a strong electric current through a tungsten wire, thereby heating it up to $2 \times 10^4$ K, and then observe the decomposition of W atoms. Since the methods of solid state mass spectrometry were not yet developed at the time, the main diagnostic objective of the experiment was the spectrum analysis of gas generated after the electric explosion of tungsten wire.

A capacitor ($C = 0.1$mkF) charged to $Vd = 35$ kV was used to create a current pulse in the experiment [1]. The high-voltage discharge switching was done using an untriggered discharger. Electric explosion of tungsten wire was conducted in a spherical bulb made of Pyrex glass. Tungsten wire, length $l = 40$ mm and diameter $d = 35$ mm, was placed "as a spacer" between the two tungsten electrodes that were sealed in the bulb at two opposite sides. In equatorial cross section, with respect to the electrodes, the "spectral" electrode was sealed. It served as one of the electrodes for the ignition of plasma discharge in the gas formed after the electric explosion.

It should be emphasized that the preparations for the experiments were carried out very carefully. Before the electric explosion of wire the inner surface of the bulb was heated in oven continuously for 15 h at $t = 300$°C simultaneously with evacuation. At the same time with the heating of the glass bulb an electric current was passed through the tungsten wire which heated it to a temperature of $\sim 2000$°C. After completion of the degassing procedure, the glass tube connecting the flask to a mercury pump was melted using a burner, and sealed.

The volume of gas generated after the EEC, averaged over the 21 shots, was $V \approx 1\,\mathrm{cm}^3$ (under normal conditions), i.e. about $10^{19}$ particles. The volume of gas observed after EEC was so large that an attempt to explain its appearance due to the release of gas previously dissolved or absorbed by the wire seemed very unlikely to the authors. The average volume of gas produced was 26 500 times more than an average volume of wire (0.0381 cm$^3$).

According to the authors of this work, the spectral analysis of gas formed by electric explosion, revealed the presence of the characteristic bright-yellow line of helium ($^4$He) in all of the experiments. Another no less important statement was the fact that the spectral analysis did not show any characteristic lines of hydrogen. This fact indicates the exceptional care taken in these experiments because, it is well known, getting rid of water vapor on the chamber glass walls and hydrogen dissolved in a tungsten wire is a very difficult task. Moreover, according to the authors, they also observed but did not identify two lines in the red part of the spectrum, a bright line in the blue part and a pale purple line. In certain experiments, the presence of two additional weak yellow lines was observed. The authors of [1]

interpreted the results of the experiment as a confirmation of their hypothesis. In modern terms their conclusion was that with the help of a high-current EEC it is possible to initiate $\alpha$-decay of one or more isotopes of tungsten nuclei.

It is quite understandable that the publication [1] caused a reaction in the scientific community of the time. Rutherford expressed deep doubts that the voltage (about 30 kV) used in the experiment was sufficient to ensure that the electrons could induce nuclear reactions. To check the reliability of the published results, Rutherford used a 100 kV electron beam on a tungsten target. He directed a beam on the target and did not observe any nuclear reactions. He described this in a short message [3] in quite a harsh form. Wendt entered into scientific discussion with Rutherford, noting that the cause of discrepancies in the results could be the difference in the power input to the tungsten target [4]. The power dissipated in the wire during the capacitor discharge and the amount of current flowing through it is much greater than the one which was used by Rutherford in his electron beam. The scientific community took Rutherford's side, and the work [1] was considered erroneous and was forgotten.

In subsequent decades, dozens of research groups [5–9] studied the electric explosion of wires. To date, the generally accepted opinion in the scientific community is that in a high-temperature plasma that occurs in powerful EEC, only nuclear fusion reactions can take place (such as D +D); i.e. the processes that occur with the participation of strong nuclear interactions. Therefore, the focus of the EEC experimental studies has been to measure the neutron flux [10] and the soft X-ray radiation [11,12]. Scientists studied the electric explosions of tungsten wires very carefully, and because no one has ever reported the observation of the spectral lines of helium, at first glance it may seem that Rutherford was right and there is no effect. On the other hand, we have not managed to find any publication which reported the chemical composition of the gas which forms in the explosion chamber at the moment of EEC.

Even though the original hypothesis of Wendt and Irion appears deeply flawed today, considering the care with which they conducted the experiment [1] we decided to test their results using modern diagnostic methods and relying on modern theoretical concepts.

## 2. Modern Theoretical Concepts

First of all, it should be noted that for all five isotopes of tungsten $\alpha$-decay is an energetically favorable process. Moreover, quite recently the half-life of one of the tungsten isotopes was $^{180}W : T^1/_2 = (1.8 \pm 0.2) \times 10^{18}$ years [13]. Thus, if we assume that the results of [1] are not wrong, they do not directly contradict the law of conservation of energy, but significantly contrary to the laws of probability. According to the classical theory of $\alpha$-decay, the probability of $\alpha$-decay is proportional to the product of the probability of $\alpha$-particle formation inside the nucleus at its surface and the likelihood $P_\alpha$ of subsequent $\alpha$-particle tunneling through a potential barrier $D_\alpha$. The probability of $\alpha$-particle formation, in the framework of the shell model of the nucleus, is calculated as the square of the matrix element of transition M$\alpha$ from the initial kernel state into a state where four nucleons form $\alpha$-particle [14]. Calculating the probability of quantum particle tunneling through a potential barrier is a classical problem of quantum mechanics. It consists of finding the distribution of the wave function of $\alpha$-particle, which is the solution of the Schrodinger wave equation of quantum particle motion in the pit, the walls of which is a field of nuclear forces and the Coulomb potential.

For a long time, it was believed that the $\alpha$-decay probability is determined solely by strong nuclear forces, and the form of the Coulomb potential does not affect the $\alpha$-decay probability. However, in 1957, Erma published a theoretical article [15], in which he showed that the presence of electrons in the atom increases the $\alpha$-decay probability compared to the $\alpha$-decay probability of fully ionized atoms.

First, the field of atomic electrons reduces the barrier for $\alpha$-particle; and, secondly, the charge of the nucleus decreases by two units during $\alpha$-decay, resulting in a change in the energy of the electron shell. Accounting for the effects of the atomic electrons leads to the fact that in calculating the $\alpha$-decay constant the energy of $\alpha$-particle should be replaced by "efficient" energy, which is greater than real $E \to E + 73Z^{4/3} + 65Z^{5/3}$ eV. Because of the exponential dependence of the probability of $\alpha$-decay from $\alpha$-particle energy, the impact of the atomic electrons can be significant.

In other words, it is much easier for the quantum particle to overcome a "high", but "narrow" barrier rather than a "low", but "wide" one. As expected, the atomic electrons have stronger influence on the processes taking place with small energies. For example, for the $^{147}$Sm ($\alpha$-particle energy $\sim$ 2.31 MeV; $T1/2 = 7\times10^{11}$ years) the presence of the electron shell increases the probability of $\alpha$-decay by 2.6 times compared with the nucleus of a fully ionized atom [15].

From the results of [15] it follows that the probability of $\alpha$-decay can be increased with the help of external electromagnetic influences, such as the application of a strong magnetic field. Influence of superstrong magnetic field on the probability of $\alpha$-decay can be qualitatively described as follows. An external superstrong magnetic field, due to the deformation of the electron shell, changes both the spatial distribution of the electric potential and energy of the electron shell of an atom and, therefore, the energy of any nuclear decay, because the decay energy is equal to the difference of the total energies of the initial and final systems, taking into account the ionization energies of atoms or ions. The role of these factors was analyzed in more detail in [16–18].

In 1970, experimental work was published [19] from which it followed that the violation of spatial parity was observed during $\alpha$-decay of $^{16}$N. Since the violation of spatial parity is a characteristic property of weak nuclear interactions, the results of the experiment [19] clearly indicate that $\alpha$-decay phenomenon involves all three types of interactions: electromagnetic, weak and strong nuclear interactions. Since the constant of the weak nuclear interaction $\alpha$ w is considerably less than the constant of electromagnetic interaction $\alpha$e, this indicates, at least in principle, the possibility of indirectly initiating of $\alpha$-decay, due to the influence of electromagnetic processes on the probability of occurrence of weak nuclear processes. Possible ways of initiation of low-energy nuclear processes, taking place with the participation of the weak interactions, are discussed in detail in [16,20].

It is well known that the probability of nuclear processes that take place with the participation of leptons (k-capture, $\beta^{\pm}$-decay) depends on the density of the real (occupied) and virtual (free, unoccupied) lepton states of the nucleus [17,18,21]. Thus, nuclear processes can be affected by changing the density of lepton states externally (by imposing external electromagnetic fields or ionizing the electron shells of the atom). Moreover, such indirect changes in the probability of nuclear processes can reach several orders of magnitude under the influence of an external electromagnetic field [22]. In [20], the possibility of participation of virtual (free, unoccupied) electron states in the process of $\alpha$-decay of heavy nuclei was discussed. In this case, a significant indirect increase in the probability of decay in superstrong electromagnetic fields is also possible due to changes in the density of these unoccupied electron states at the core.

Another, hypothetical decay channel, leading to the induced decay of heavy nuclei, is an energetically favorable process of $\alpha$-decay that occurs simultaneously with $\beta$-decay ("$\alpha\beta$-decay").

$$^{A}_{Z}\mathrm{X} \rightarrow {}^{A-4}_{Z-1}\mathrm{Y} + {}^{4}_{2}\mathrm{He} + e^{-} + \bar{\nu} + Q,$$

where X and Y – a nuclei with atomic weight A and $(A-4)$ and charges $Z$ and $(Z-1)$, respectively, $\bar{\nu}$ – antineutrino, $Q$ – the released energy. For example:

$$^{163}_{66}\mathrm{Dy} \rightarrow {}^{159}_{65}\mathrm{Tb} + {}^{4}_{2}\mathrm{He} + \mathrm{e}^{-} + \bar{\nu} + 0.70\,\mathrm{MeV},$$

$$^{181}_{73}\mathrm{Ta} \rightarrow {}^{177}_{72}\mathrm{Hf} + {}^{4}_{2}\mathrm{He} + \mathrm{e}^{-} + \bar{\nu} + 2.02\,\mathrm{MeV},$$

$$^{183}_{74}\mathrm{W} \rightarrow {}^{179}_{73}\mathrm{Ta} + {}^{4}_{2}\mathrm{He} + \mathrm{e}^{-} + \bar{\nu} + 1.57\,\mathrm{MeV},$$

$$^{184}_{74}\mathrm{W} \rightarrow {}^{180}_{73}\mathrm{Ta} + {}^{4}_{2}\mathrm{He} + \mathrm{e}^{-} + \bar{\nu} + 0.80\,\mathrm{MeV},$$

$$^{186}_{74}\mathrm{W} \rightarrow {}^{182}_{73}\mathrm{Ta} + {}^{4}_{2}\mathrm{He} + \mathrm{e}^{-} + \bar{\nu} + 1.50\,\mathrm{MeV},$$

$$^{201}_{80}\mathrm{Hg} \rightarrow {}^{197}_{79}\mathrm{Au} + {}^{4}_{2}\mathrm{He} + e^{-} + \bar{\nu} + 1.05\,\mathrm{MeV}.$$

**Table 1.** Isotopes for which $\alpha\,\beta$-decay is energetically favorable.

| Initial nucleus | | | Product of $\alpha\beta$-decay | | | Energy of $\alpha\beta$-decay (keV) | Energy of $\alpha$-decay (keV) | Energy of $\beta$-decay (keV) |
|---|---|---|---|---|---|---|---|---|
| Name | Z | A | Name | Z | A | | | |
| La | 57 | 138 | Ba | 56 | 134 | 0.59 | –2057 | 1045 |
| Nd | 60 | 145 | Pr | 59 | 141 | 2159 | 1578 | –164 |
| Nd | 60 | 146 | Pr | 59 | 142 | 437 | 1182 | –1470 |
| Nd | 60 | 148 | Pr | 59 | 144 | 917 | 597 | –540 |
| Nd | 60 | 150 | Pr | 59 | 146 | 651 | –415 | –87 |
| Pm | 61 | 145 | Nd | 60 | 141 | 499 | 2321 | –615 |
| Sm | 62 | 147 | Pm | 61 | 143 | 1269 | 2311 | –1720 |
| Sm | 62 | 149 | Pm | 61 | 145 | 1707 | 1870 | –691 |
| Eu | 63 | 151 | Sm | 62 | 147 | 2189 | 1963 | –463 |
| Eu | 63 | 153 | Sm | 62 | 149 | 1345 | 272 | –485 |
| Gd | 64 | 155 | Eu | 63 | 151 | 158 | 79 | –822 |
| Gd | 64 | 157 | Eu | 63 | 153 | 118 | –689 | –59 |
| Tb | 65 | 159 | Gd | 64 | 155 | 113 | –140 | –366 |
| Dy | 66 | 161 | Tb | 65 | 157 | 284 | 343 | –859 |
| Dy | 66 | 163 | Tb | 65 | 159 | 727 | –242 | –1.42 |
| Ho | 67 | 165 | Dy | 66 | 161 | 733 | 138 | –376 |
| Er | 68 | 167 | Ho | 67 | 163 | 663 | 666 | –747 |
| Er | 68 | 170 | Ho | 67 | 166 | 537 | 51 | –313 |
| Tm | 69 | 169 | Er | 68 | 165 | 824 | 1201 | –908 |
| Yb | 70 | 171 | Tm | 69 | 167 | 811 | 1557 | –1479 |
| Yb | 70 | 173 | Tm | 69 | 169 | 1297 | 946 | –671 |
| Yb | 70 | 174 | Tm | 69 | 170 | 426 | 738 | –1357 |
| Yb | 70 | 176 | Tm | 69 | 172 | 1462 | 571 | –105 |
| Lu | 71 | 175 | Yb | 70 | 171 | 1716 | 1619 | –685 |
| Lu | 71 | 176 | Yb | 70 | 172 | 3448 | 1568 | 1192 |
| Hf | 72 | 177 | Lu | 71 | 173 | 1574 | 2245 | –1166 |
| Hf | 72 | 178 | Lu | 71 | 174 | 709 | 2084 | –1912 |
| Hf | 72 | 179 | Lu | 71 | 175 | 2276 | 1807 | –109 |
| Hf | 72 | 180 | Lu | 71 | 176 | 1177 | 1281 | –854 |

Table 1 continued

| | | | | | | | | |
|---|---|---|---|---|---|---|---|---|
| Ta | 73 | 180 | Hf | 72 | 176 | 3224 | 2029 | 708 |
| Ta | 73 | 181 | Hf | 72 | 177 | 2024 | 1524 | –188 |
| W | 74 | 183 | Ta | 73 | 179 | 1571 | 1682 | –556 |
| W | 74 | 184 | Ta | 73 | 180 | 804 | 1657 | –1483 |
| W | 74 | 186 | Ta | 73 | 182 | 1496 | 1123 | –580 |
| Re | 75 | 185 | W | 74 | 181 | 2007 | 2195 | –1013 |
| Os | 76 | 187 | Re | 75 | 183 | 2165 | 2720 | –1501 |
| Os | 76 | 188 | Re | 75 | 184 | 660 | 2143 | –2808 |
| Os | 76 | 189 | Re | 75 | 185 | 2409 | 1974 | -533 |
| Os | 76 | 190 | Re | 75 | 186 | 797 | 1377 | -2000 |
| Os | 76 | 192 | Re | 75 | 188 | 711 | 362 | –1045 |
| Ir | 77 | 191 | Os | 76 | 187 | 2086 | 2084 | –1019 |
| Ir | 77 | 193 | Os | 76 | 189 | 2027 | 1016 | –55 |
| Pt | 78 | 195 | Ir | 77 | 191 | 1472 | 1158 | –225 |
| Pt | 78 | 198 | Ir | 77 | 194 | 184 | 87 | –324 |
| Au | 79 | 197 | Pt | 78 | 193 | 898 | 953 | –600 |
| Hg | 80 | 199 | Au | 79 | 195 | 598 | 823 | –1445 |
| Hg | 80 | 201 | Au | 79 | 197 | 1053 | 333 | –483 |
| Hg | 80 | 204 | Au | 79 | 200 | 148 | –512 | –346 |
| Tl | 81 | 203 | Hg | 80 | 199 | 1363 | 909 | –974 |
| Tl | 81 | 205 | Hg | 80 | 201 | 1419 | 143 | –51 |
| Pb | 82 | 207 | Tl | 81 | 203 | 883 | 390 | –2399 |
| Pb | 82 | 208 | Tl | 81 | 204 | 171 | 519 | -2879 |
| Bi | 83 | 209 | Pb | 82 | 205 | 3086 | 3138 | –1893 |
| Th | 90 | 232 | Ac | 89 | 228 | 4129 | 4082 | -495 |
| U | 92 | 234 | Pa | 91 | 230 | 3549 | 4858 | –1809 |
| U | 92 | 235 | Pa | 91 | 231 | 5068 | 4678 | –123 |
| U | 92 | 238 | Pa | 91 | 234 | 4543 | 4269 | –145 |

For such types of decays, as well as for classical $\beta$-decays, one can expect a significant increase in the probability of decay when an atom is exposed to an external superstrong magnetic field. However, even if individually $\alpha$- and $\beta$-decays (e.g., for the core) are energetically forbidden, the simultaneous "$\alpha\beta$-decay" can be an energetically favorable process. The essential difference of the process from the classical $\alpha$-decay is as follows: in $\alpha\beta$-decay total energy (i.e. mass sum and kinetic energy) of the final nucleus ${}^{A-4}_{Z-1}\mathrm{Y}$ and the $\alpha$-particle is always smaller than the mass of the compound nucleus ${}^{A}_{Z+1}\tilde{X}$ . For example, for the first decay the sum of energies of $\alpha$-particle and the ${}^{159}_{65}\mathrm{Tb}$ is less than the mass of ${}^{163}_{67}\mathrm{Ho}$ nucleus. It obviously follows from the fact that the original nucleus is $\beta$-stable. That is, an artificial combination of $\alpha$-particle and the ${}^{159}_{65}\mathrm{Tb}$ nucleus cannot give a real ${}^{163}_{67}\mathrm{Ho}$ nucleus – obtained nucleus can only be "virtual", with energy lesser than the energy of the ground state for ${}^{163}_{67}\mathrm{Ho}$ nucleus.

All stable isotopes, for which $\alpha\beta$-decay is energetically favorable, are shown in Table 1. The table shows: the decaying isotope, decay product and energy of $\alpha\beta$-decay. The sign "–" in the line of energy means that process is energetically unfavorable, and hence its absolute prohibition.

Although the probability of such a process is very low in normal conditions, a superstrong magnetic field may be

a good "catalyst." Since, in a superstrong magnetic field, the phase volume of bound states of electrons, in which the $\beta$-decay can occur, significantly increases [22]. The magnetic field "pulls out" the electron, which, for these isotopes, can be born only with the departure of an $\alpha$-particle: i.e. a "torn out" $\alpha$-particle provides the necessary energy. The development of $\alpha\beta$-decay theory and calculation of the process probability is similar to the calculation of the probability of forbidden $\beta$-decays [22], but the nuclear function of the final state should include the birth of an $\alpha$-particle. Note that, for $\beta$-decay of nucleus in a superstrong magnetic field, the electron will be born in a bound state.

As mentioned above, the $\alpha\beta$-decay process is fundamentally different from the classical $\alpha$-decay in that it occurs through the formation of an intermediate nucleus, the energy of which is less than the energy of the ground state of the nucleus ${}^{A}_{Z+1}\tilde{X}$. Since the intermediate nucleus formed from an $\alpha$-particle and final nucleus ${}^{A-4}_{Z-1}\mathrm{Y}$ is virtual, the wave functions of the $\alpha$-particles produced during the $\alpha\beta$-decay and during classical $\alpha$-decay differ greatly. In case of classical $\alpha$-decay the wave function of $\alpha$-particle describes the virtual particle in the potential barrier, but a real one both outside and inside the nucleus. In the test problem of the wave function of $\alpha\beta$-decay the energy of $\alpha$-particle inside the nucleus should be less than the potential energy inside a nucleus. That is, in contrast to the classical $\alpha$-decay the wave function $\Psi$ of $\alpha$-particle will describe a real particle outside of the nucleus, but virtual, both inside the barrier and in the nucleus inner region. Thus, $\alpha$-particle is created virtual [20].

Since, similar to the classical $\beta$-decay, the lepton (electron and neutrino) wave functions do not change significantly at the distances of the order of size of the nucleus, the lepton factor can be taken outside the integral of the nuclear matrix element. Integrands of nuclear matrix elements that depend on the spatial coordinates can always be represented as an expansion in orthonormal spherical functions. In this case (as in the case of classic $\beta$-decay [22]), when the square of the matrix element is calculated, the nuclear part of the matrix element can be taken out outside the summation sign of the lepton states, and the square of each element of the matrix will be equal to:

$$|M_i|^2 = |M_{Ni}|^2 f_s(ZQ),$$

Where $M_{Ni}$ is the corresponding first non-zero moment of the nuclear part of the matrix element, $f_s \,\mathrm{is\,the}$ Fermi integral function, which determines the phase volume of the final lepton states, $Q$ is the energy of the nuclear transition. An "explosive" increase in the lepton phase volume $f$ occurs, when an external superstrong (on the atomic scale) magnetic field is applied to an atom, due to the increase in the density of free states of electrons of the discrete spectrum. It can be assumed that these magnetic fields are small compared to "nuclear" level, and the nuclear part of the matrix elements remain practically unchanged. In [22] electron wave functions are calculated in cylindrical coordinates in an external static uniform superstrong magnetic field and in the central electric field of the nucleus, and the spectrum of bound states of electrons is shown. The sum of the lepton phase volume (i.e. the density of electron states in the area of the nucleus) over all electronic states of the discrete spectrum is proportional to $\Sigma_\chi(B_\chi/\chi)$, where $\chi$ is the quantum number of the longitudinal state (along the magnetic field) in which the electron is born and $B_\chi$-coefficients which are determined by the form of the solution of the electron equation in the central electric and static uniform magnetic fields (where the exact solution is given in [22]). The reason why the electron density is inversely proportional to the degree of longitudinal quantum number in a superstrong magnetic field lies in the fact that influence of a superstrong magnetic field on the atom reduces spherical symmetry to the one-dimensional Coulomb problem. In the superstrong magnetic field electron orbit transformed into the cylinders stretched along the magnetic field with a transverse dimension equal to the Larmor radius and a longitudinal dimension equal to the Bohr radius (which is proportional to the quantum number $\chi$ of longitudinal motion). Formally, this sum diverges at large $\chi$ ($B_\chi$factors are limited from below), it shows that the excited states of longitudinal motion provide the main contribution to the $\beta$-decay probability.

For the allowed and the unique-forbidden $\alpha\beta$-decay, among matrix elements only one is dominant and, in these cases, it is obvious that the probability of decay is proportional to the square of this matrix element. Thus, the proba-

bility of decay is proportional to the Fermi function $f$, which, in turn, in superstrong magnetic field, is proportional to the phase volume of bound states of electrons and neutrinos. Since the phase volume of the neutrino is proportional to the square of the neutrino energy, then for the decay to a bound state of the electron, the probability of such decay is proportional to the square of the energy $Q$ released during the nuclear reaction [22]:

$$\lambda_{\alpha\beta} \propto Q^2 \sum_{\chi} \left( \frac{B_\chi}{\chi} \right).$$

For the forbidden (non-unique) decays among matrix elements there are those that will have close values, and the probability of decay will be calculated in a more complicated way. But, in any case, you can always use this expression for a rough estimation.

Thus, we can see that in a superstrong magnetic field, the Larmor radius of the electron becomes small compared to the Bohr radius, and the phase volume of unoccupied lepton states increases infinitely, i.e. the so-called "burst phase volume" is observed [22]. This leads to an increase in the number of final states of the system, in which the decay may occur, which, in turn, leads to an increase in the probability of nuclear decays with the birth of an electron. Energetically favorable nuclear processes, in which $\alpha$-decay occurs at the same time with $\beta$-decay to a bound state ("$\alpha\beta$-decay"), can acquire a finite probability in a superstrong magnetic field due to "an explosion of lepton phase volume."

As seen from the above, our understanding of nuclear physics have changed considerably over the past 90 years, and today, Rutherford's point of view no longer appears to be as inviolable as before. Of course, the above arguments in favor of the possibility of initiating $\alpha$ decay via influence of a superstrong magnetic field on the heavy atoms are purely theoretical and the probability of such processes are very small, but it is important that their implementation is not forbidden by the conservation laws. The possibility of initiating nuclear processes that occur with the participation of weak nuclear interactions, with the help EEC, has not yet been investigated experimentally.

## 3. Experimental Section

Experiments on electric explosion of a tungsten wire were conducted in 2010–2011 at the Sukhumi Institute of Physics and Technology (The Republic of Abkhazia) with the "HELIOS" experimental setup.

### 3.1. Description of the experimental setup and procedure for conducting experiments

The electrical part of the setup consists of four IMN 100-0.1 capacitors with capacitance $C = 0.1\mu$ F and an inductance of 150 nH connected in parallel. To reduce the total inductance, the bus of capacitors is made of sheet copper 1 mm thick. Charging was performed by an AII-70 power supply unit through a rectifier and a charging resistor to the voltage $U = 35{-}40$ kV.

The capacitor bank was closed using a three-electrode low-inductance controlled air discharger. The discharger was connected to the explosion chamber by eight parallel radiofrequency cables ($\rho = 50\,\Omega$, $L = 200$ nH/m) two meters long each.

A schematic diagram of the vacuum system of the setup is shown in Fig. 1. Vacuum pumping of the chamber (6) was carried out with an oil-free spiral vacuum pump Varian SH-110 (1) and a turbo-molecular pump 01AB-450-003 (14) (with the limit of $4 \times 10^{-5}$ Pa) up to the pressure $\sim 10^{-4}$ Pa.

The explosion chamber (6) was attached to the vacuum gate (10) via an intermediate flange 25 mm height and 120 mm in diameter (9) which has a center hole for vacuum pumping. At the same time, the flange (9) served as the place connecting to the FRG700 pressure sensor and devices for the study of the gas mixture resulting after the EEC. The joint for the leak valve (7) was located in the upper flange of the explosion chamber coupler. The leak valve

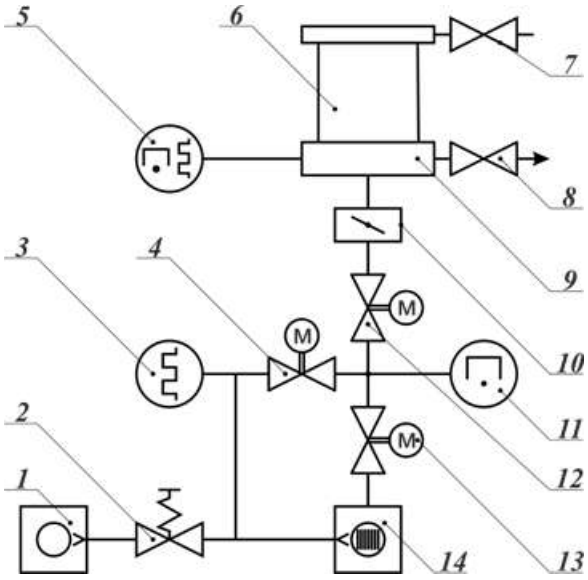


**Figure 1.** Diagram of the vacuum system. 1 – backing pump Varian SH-110; 2 – off valve; 3 – manometer gauge Pirani PMT-6; 4, 12, 13 solenoid valves type KEUN-40; 5 – combined full-range vacuum sensor Varian FRG700; 6 – blast chamber; 7 – manual "fine" leak valve; 8 – valves for connection of gas diagnostics; 9 – intermediate flange; 10 – manual gate valve type Varian VGA0631M; 11 – manometric sensor PMM-32; 14 – turbo molecular pump TMP 01AB-450-003.

(7) served as the inlet for air, calibration gas mixtures or “service” gas required for cleaning the inner surface of the chamber.

In the experiments described here, two types of explosion chambers were used: drawn quartz tube (inner diameter 55 mm, height 110 mm, wall thickness of 2–3 mm) and a stainless steel cylinder ($^{12}$Cr$^{18}$Ni$^{10}$Ti, internal diameter 55 mm, height 110 mm, wall thickness 2.5 mm). The volume of explosion chamber itself was $V_{\rm chamber} \approx 250$ cm$^3$ and the total volume to the place of the gate setup, including all the technological appendages, $V_{\rm sum} = 397 \pm 4$ cm$^3$. The value of the total volume $V_{\rm sum}$ is very important for a correct measurement of the absolute number of particles with $m = 4$. The following procedure was used to precisely measure the total volume. A pre-evacuated calibration tank, with the precisely measured volume $V_{\rm cal}$, was joined to the closed valve 5 (Fig. 2). Then, with gate 10 closed and valve 5 opened, the chamber was filled with gas, the pressure of which was controlled by a digital gauge. After that, the valve on the calibration tank was opened and the pressure equalized in both volumes $V_{\rm sum}$ and $V_{\rm cal}$. After closing the gate 5, calibration tank was disconnected and evacuated, and then the procedure was repeated several times. By controlling the amount of pressure on each step of the procedure, and assuming that temperature is constant, it is quite simple to calculate $V_{\rm sum}$, and multiple repetition of procedure reduces the measurement error.

Figure 2a shows a schematic of explosion chamber, and Fig. 2b shows a photo of it. Contact between the electrodes (1) and the wire (4) was provided by a collet seal. In experiments electrodes made of tungsten and stainless steel were used. Using the latter promoted reduction of electron emission from the electrode surface, which improved the reproducibility of the results. Tungsten wires (4) of different cross sections (10, 50, 70, 130 and 200 $\mu$m) and length ranging from 24 to 40 mm were used in these experiments. In test experiments iron (Fe) wires of the same dimensions were exploded.

In order to reduce the amount of gas adsorbed by the walls of the explosion chamber, before the electric explosion,

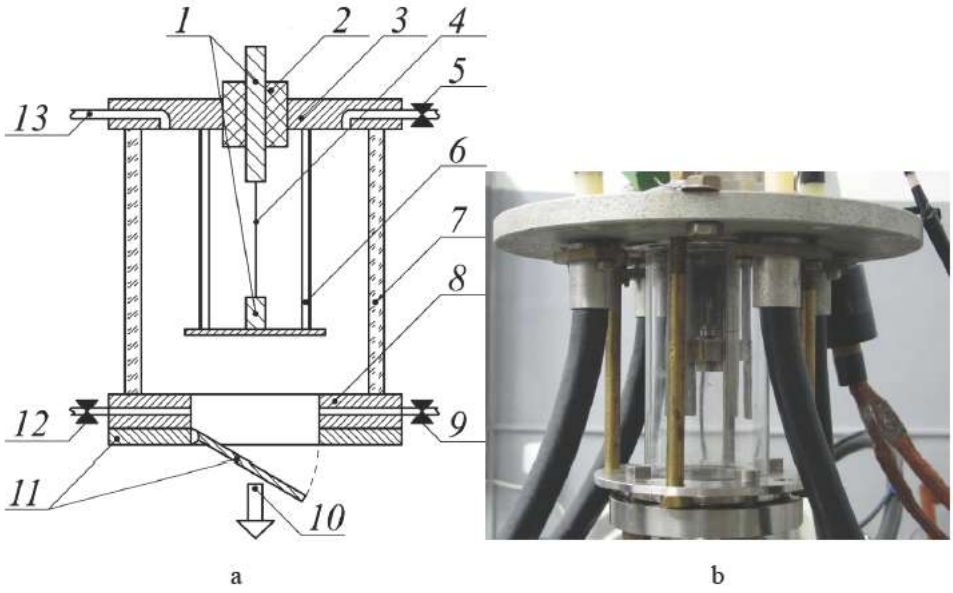


**Figure 2.** Blast chamber: (a) 1 – mounting electrodes; 2 – insulator; 3 - top flange; 4 – wire; 5 – leak valve for the inlet of argon; 6 – current-return pathway; 7 – chamber wall; 8 – lower flange; 9 – valve for MS-200; 10 vacuum pumping; 11 – gate; 12 – MS-40 valves; 13 – hole for pressure lamp connection. (b) photo of the quartz blast chamber.

the chamber was filled with argon and it was ignited with the high-frequency glow discharge. Then chamber was pumped out to the required pressure using a vacuum pump. In order to degas the tungsten wire before the EEC it was heated by the current of 0.2–2 A (depending on wire diameter) to the temperature ∼1500 K for 0.5–2 h. The source for wire heating was inductively decoupled from the setup, which allows us to trigger the electric explosion without turning off the heating (hereinafter referred to as a "hot start"). The electric explosion of a tungsten wire was produced in the explosion chamber, which was cut off from the vacuum system immediately before the electric pulse. This technique allowed us to investigate the gas produced by EEC of tungsten wire. Preparations for the electric explosion were carried out in the following order:

(1) Setting the wire in the load node (coaxial assembly).
(2) Setting the load node in explosion chamber.
(3) Cleaning the chamber using glowing discharge in argon.
(4) Vacuum pumping of the chamber up to the pressure about $1 - 2 \times 10^{-5}$ Pa.
(5) Degassing the wire by heating it.
(6) Slowly turning off wire heating.
(7) Cutting off vacuum chamber from pumping system.
(8) Conducting electric explosion.
(9) Analysis of the resulting gas medium.

The time interval *t* between entries 7 and 8 was $t \leq 10$ s.

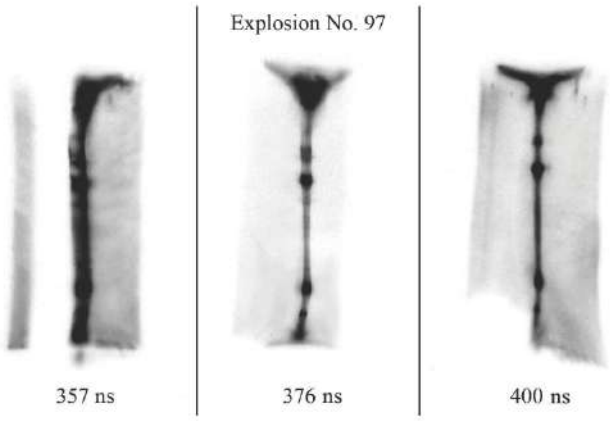


a

**(a) Typical IIT photo**

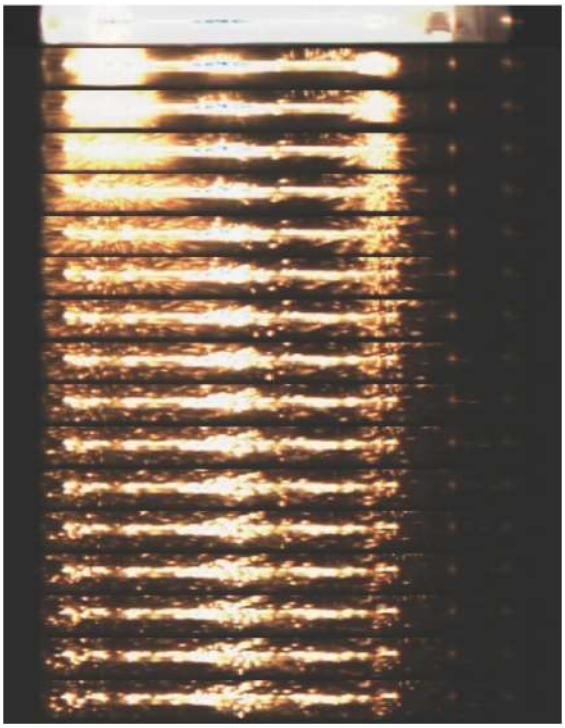

b

**(b) Set of frames from high-speed camera**

**Figure 3.** Photorecording diagnostics: (a) Typical IIT photo. (b) Set of frames from high-speed camera.

### 3.2. Main diagnostic method

All diagnostic methods that were used in the experiment can be divided into four groups: electrical, photorecording, optical and gas diagnostics.

#### 3.2.1. *Electrical diagnostics*

Electrical diagnostics were used to monitor the parameters of electric explosion. The sensors that were used included: a voltage divider, Rogowski coil and current loops. That is quite a common set of sensors which are always used in experiments of this type.

#### 3.2.2. *Photorecording diagnostics*

Equipment used as photorecording diagnostics included: a high-speed video camera with a frame rate up to 10 kHz and a three-frame electron-optical system (three image intensifier tubes, IIT) which was photographing with an exposure time $\tau \sim 15$ ns. The time delay between shots can be changed.

The high-speed video camera allowed us to control the dynamics of the explosion as a whole and three-frame IIT system provided control of emission uniformity along the length. A typical IIT photo sequence is presented in Fig. 3a. Figure 3b presents a set of frames from the high-speed video camera obtained in one of the experiments. Figure 3a shows the inhomogeneity of emission along the length of the wire and the emergence of the so-called "hot spots".

Figure 3b shows that complete destruction of the wire core takes place only by the end of the second millisecond. The fact that the wire core exists much longer than the current pulse duration was known long ago, but the application of high-speed video camera allowed us to clearly verify this. Using this same technique, it was possible to judge the degree of dispersion of tungsten powder formed during the destruction of the wire core. The degree of dispersion increases with decreasing the diameter of the exploded wire. Comparison of frames from the photorecording diagnostics with current waveforms showed that, under the same experimental conditions, the current and voltage waveforms vary little from experiment to experiment, but the visual dynamics of the EEC may undergo significant changes.

#### 3.2.3. *Optical diagnostic*

The main objective of the optical diagnostics was to obtain information on parameters and the chemical composition of the plasma formed as a result of EEC [23]. The time behavior of the integral (over the wavelength) light intensity was measured using an FD-263-01 silicon photodiode with amplifier. The signal from this device was sent to a Tektronix TDS-2024B digital oscilloscope. It should be noted that the data obtained by a photodiode served as a more reliable marker of reproducibility of experiments than the current–voltage characteristics of the electric explosion.

To determine the chemical composition of the plasma at the time of the electric explosion by spectral characteristics of light radiation two types of optical spectrometers were used. The spectrometers differ in spectral resolution.

An Abbe prism is used in one of them (UM-2) as a dispersing element, which does not allow high spectral resolution, but provides sufficient optical efficiency. Its other advantage is the fact that the entire visible spectral region fits into a length of $\sim$30 mm. This size corresponds to the diameter of the image intensifier photocathode, allowing the use of an electron-optical converter (IIT) as a light amplifier. To register the intensified spectrum, we used a high-sensitivity film that was pressed against IIT fiberglass exit port or CCD array, connected by a fiberglass washer with the tube output window. Due to its high sensitivity, this spectrometer allowed us to obtain an overview spectrum of optical radiation at every electric explosion of tungsten wire.

In the other type of optical spectrometer (STE-1), a diffraction grating is used as a dispersing element. This allowed us to record the spectrum at high resolution. However, the STE-1 sensitivity was significantly worse than that of the

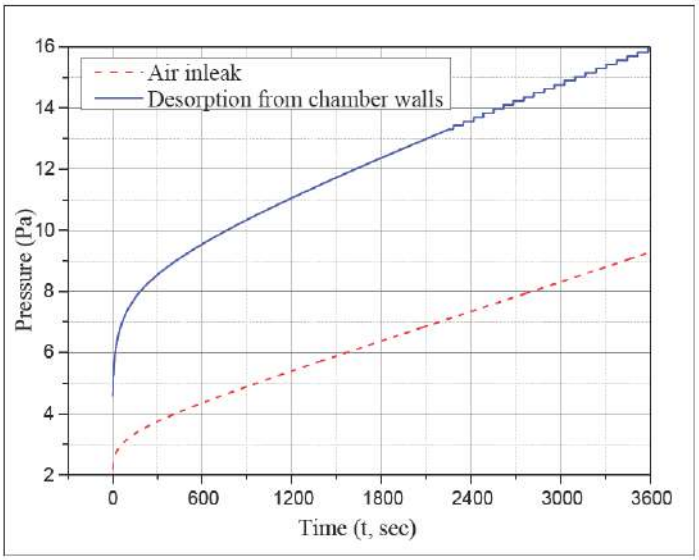


**Figure 4.** The time dependence of pressure in the chamber after the gate closing.

prism spectrometer; therefore, it was possible to measure spectra only at large light fluxes. With this instrument, we also used a CCD array as a photo-recording element and so the measured spectral range was limited by the geometrical size of the CCD array (29 mm).

### 3.2.4. *Gas diagnostic*

The specifics of the task required the study of the gas phase formed after the electric explosion. The main objectives of these methods was to identify helium atoms by weight, and to measure their quantity. As far as we know from the literature, the study of the chemical composition of the gas formed in the explosion chamber after the electric explosion of wires has never been carried out.

Registration of pressure in the explosion chamber was carried out with the help of inverted magnetron gauge VARIAN FRG-700 with an operating range $10^{-5}$–$10^{5}$ Pa. The data from the gauge was transferred to a computer, allowing us to continuously monitor the pressure changes in the setup and, therefore, evaluate gas leakage rate into the chamber with 5% accuracy in on-line mode, both before and after the electric explosion. The technique of continuous measurement of pressure played an important role in the process of preparation for the experiment (viz: wire heating, cleaning of the explosion chamber surface with glow discharge in argon, leakage elimination).

When the explosion chamber was cut off from the vacuum pumping system, the pressure increase rate in the chamber is determined by the diffusive flux from the chamber walls and inleakage of air due to imperfect sealing. However, since the diffusive flux associated with the desorption is defined as $Q_{\mathrm{d}} \sim \sqrt{t}$, and the flux associated with atmospheric inleakage is $Q_{\mathrm{at}} \sim t$ (where $t$ is the time), therefore based on the type of curve of leakage speed time dependence, it can be determined which process is dominant at a given pressure. The typical form of pressure increase time dependence after gate closing is shown in Fig. 4. If from the type of pressure increase curve it followed that diffusive flux was decisive, this was an indication for further purification of quartz chamber surface with glow discharge. If the pressure increases linearly with time, that means the determining factor is leakage from the atmosphere, and the

sealing of vacuum chamber need to be improved. Usually the level of leakage was

$$\frac{\mathrm{d}p}{\mathrm{d}t} \approx 1 \,\mathrm{to}\, 5\,\mathrm{Pa/h},$$

which made it possible to conduct EEC at a pressure $P_0$ <$10^{-3}$ Pa (including the closing time of the gate).

A compact TOF mass spectrometer (MC-200) was used for a qualitative analysis of the chemical composition of the gas formed in the explosion chamber. This was connected to valve 12 (Fig. 2). This device has resolution $R$ ~200 in investigated mass range, allowing us to confidently identify all the mass in the range of $M = 2$ to 500. In order to resolve light mass doublets ($D_2$ and $^4$He, HD and $^3$He) it was necessary to use a special device with high sensitivity and resolution $R$ ~900 in light mass region.

A helium leak detector (MS-40 DryCE; hereinafter MS-40) was used to measure the amount of gas particles with $m = 4$ a.m.u. (hereinafter $m = 4$). It was connected to the chamber via valve 9 (Fig. 2) using a short stainless steel pipe. Two parallel-connected shut-off valves, which had different throughput capacity, were mounted between the explosion chamber and pipe. Gas formed after electric explosion was pumped out first through the valve having a small hole, and further, with decreasing of pressure in the chamber, through the second valve with a larger hole. This procedure allows us to stay within the linear counting mode of the MS-40 device and correctly measure of the gas flux with $m = 4$ during the entire gas evacuation process, regardless of the initial pressure in the explosion chamber.

The MS-40 sent data to a computer, where it was processed using specially written software. The sensitivity of the device allows us to confidently detect the atmospheric helium and carry out quantitative measurements of particles with $m = 4$ starting from the flow rate $\sim 10^{10}$ at. cm$^3$ s$^{-1}$. Periodically (every 10 measurements), the MS-40 is automatically calibrated according to value of the helium flow in the built-in calibration leak (flow $\sim 3\times 10^{-8}$ bar cm$^3$ s$^{-1}$).

The following procedure was developed to calibrate the method of measuring particles $m = 4$ using the MS-40. In the explosion chamber, previously evacuated to pressure $10^{-4}$ Pa, a known amount of air was let in and then pumped through the leak detector, counting the number of $^4$He atoms. Since $^4$He concentration in the atmosphere and

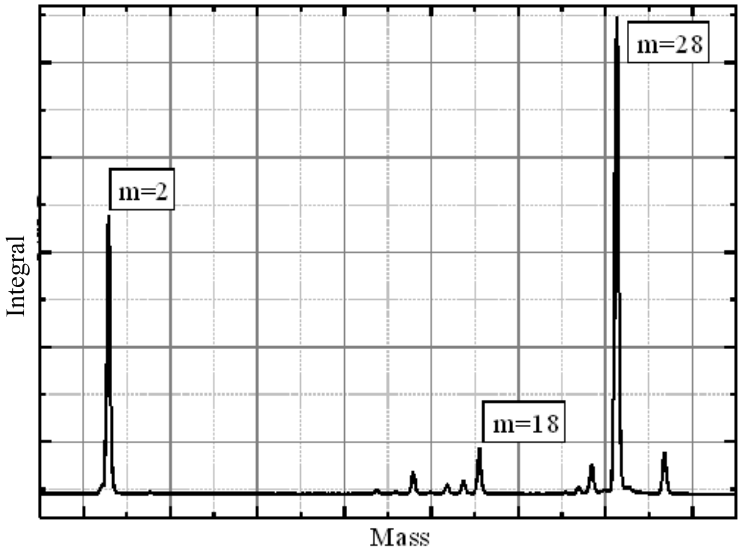


**Figure 5.** Mass spectrum of gas produced as a result of EEC.

the amount of $V_{\rm sum}$ of the chamber are known, it is possible to relate the experimentally measured quantity of $^4$He particles to theoretically calculated value for a given volume of the chamber. To account for the nonlinearity of the MS-40 ionization unit and detector, the calibration was carried out at all pressure ranges (10, 20, 50, 67 Pa, and so on), which were observed in the explosion chamber after EEC. To calibrate the MS-40 for the study of gas mixtures with $^4$He concentration higher than in the atmosphere ($\gamma = 5 \times 10^{-6}$) calibration gas mixtures with a known concentration of 4 $^4$He were created. A special stand was designed to create such calibration mixtures. These efforts have allowed to use the MS-40 device as a measurement tool.

Due to its low mass resolution, the leak detector cannot distinguish $D_2$ molecule from $^4$He atom, which creates uncertainty in the results obtained. Spectral optical methods were designed to eliminate this uncertainty.

There were attempts to detect fast neutrons. Neutron search methodology was based on the registration of the recoil protons. An organic scintillator detector (diameter 40 mm and length 60 mm) combined with PMT was used for that purpose. However, no signals indicating the birth of neutrons at the moment electric explosion had been recorded during the experiments.

### 3.3. Experimental results

#### 3.3.1. *Gas diagnostic*

Pressure of about $P_1$ ∼50 Pa was observed in the chamber after EEC, which correlates well with the results of [1]. Chemical analysis of the gas, resulting from the electric explosion, conducted using an MS-200 mass spectrometer [24] showed that the gas consists of about 40% hydrogen and the remaining 60% is a gas mixture that is similar in chemical composition to air. As can be seen from the typical gas mass spectrum shown in Fig. 5, the peaks $m = 2$ a.m.u. (hydrogen molecule $H_2$) and $m = 28$ a.m.u. (molecules of nitrogen $N_2$ or carbon monoxide CO) are prevalent in the spectrum. However, considering the fact that the peak of $m = 14$ a.m.u. (nitrogen atom N) and the peak of $m = 32$ a.m.u. (oxygen molecule $O_2$) are relatively small, we can confidently say that the peak of $m = 28$ a.m.u. is a gas mixture of nitrogen and carbon monoxide. Peaks of water and its "fragments" ($H_2O$, OH, O), which are always present in any mass spectrometry equipment, are also visible in the spectrum. This is due to the fact that water molecules are adsorbed by the surface very easily.

The pressure surge and chemical composition of the gas depend weakly on the wire parameters (its radius and length). This means that the major contribution to the gas phase EEC was conditioned by degassing of the chamber walls and other structural elements. One way to reduce the amount of degassed particles is to increase the damping coefficient of the discharge circuit. A non-linear resistance (depending on temperature) was mounted between the cables, which conveying the pulse from the battery to the load, and the wire to achieve an aperiodic current pulse. Figure 6 shows current waveforms of experiments with different modes: oscillating current (Run No. 147) and almost aperiodic current pulse (Run No. 109). With the same dimensions of the W wire, in experiments with low $Q$-value of the circuit, gas pressure after EEC averaged over a series of five experiments, was PL $= 22 \pm 2$ Pa and in experiments with a high $Q$-value of the circuit pressure was PH $= 61 \pm 5$ Pa. Comparing obtained pressure values with current waveforms we can conclude that more than half of the total gas is produced after the passage of the first half period of the current, i.e., by oscillating discharge.

The peak in the area of $m = 3$ a.m.u. is barely noticeable in the mass spectrum presented in Fig. 5. Figure 7 shows a magnified fragment of mass spectrum where a peak with $m = 3$ a.m.u. is clearly visible. Due to the fact that the MS-200 mass-spectrometer does not have sufficient resolution, the $m = 3$ peak may be interpreted as: HD molecule, the hydrogen ion, hydrogen isotope $^3$H and helium isotope $^3$He. The presence of tritium $^3$H in the experiment seems unlikely, as there no significant level of radioactivity was detected. It is also difficult to attribute peak $m = 3$ to hydrogen ions because such ions lifetime very small compared to the measurement time. The possibility of formation of such ion in the mass spectrometer ionizer is negligible [25]. Thus, the peak of $m = 3$ a.m.u. in the spectrum can

be associated with the appearance of either HD molecules, or with $^3$He atoms. It should be noted that MS-40 has an option for measuring the number of particles with $m = 3$, but our inability to carry out the calibration, due to the lack of $^3$He calibration source, did not allow us to use the MS-40 function to count the number of particles with $m = 3$.

The sources of hydrogen could be: water that remained on the metal surfaces; Viton gaskets used for sealing or hydrogen, which did not completely diffused during the heating of tungsten wire. Based on the research we performed it is difficult to clearly indicate the origin of such a large amount of hydrogen. But since there is a noticeable amount of water fragments in the mass spectrum, it can be argued that a significant portion of hydrogen owes its origin to the water remained on the chamber walls. The ratio between normal water $H_2O$ and semi-heavy water DHO is about 3500: 1. Approximately the same ratio is valid for the $H_2$ and HD gases, therefore the same ratio between the peak amplitudes of the second and third mass peaks should be expected in gas mass spectrum. However, the ratio between these peaks, in the experiments, was in the range of 30–200:1.

The MS-200 mass-spectrometer is able to record the time dependence of values of the ion currents for selected masses. The time dependence of peaks $m = 2$ and $m = 3$ is shown in Fig. 8. Assuming that the presence of peak $m = 3$ is associated with the molecules of HD, time dependence of peaks $m = 2$ and $m = 3$ should correlate, since both peaks are caused by the presence of hydrogen in the measured gas mixture. As it can be seen from Fig. 8 $m = 3$ peak quickly disappears and the time trend of peaks $m = 2$ and $m = 3$ does not correspond to our assumption. Thus, the experimental data indicates that the appearance of a peak with $m = 3$ a.m.u. can be associated with the formation of $^3$He. Since the optical spectra of $^3$He and $^4$He are very similar, such a conclusion does not contradict the results of [1], but it is significantly contrary to theoretical considerations expressed in our article.

The method of continuous measurement of total pressure was very helpful during the counting the number of $m = 4$ particles contained in the explosion chamber with the help of MS-40 leak detector, as it allowed, with good accuracy, to consider the number of $^4$He leaked into the explosive chamber from the air in the atmosphere.

The procedure for measuring the number of $m = 4$ particles was as follows. After the electric explosion all the gas located in the explosion chamber was pumped through a helium leak detector, which allow us to calculate the total

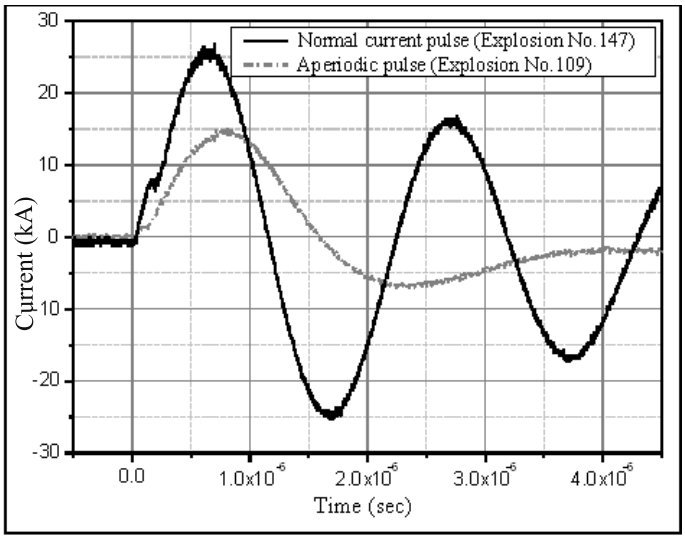


**Figure 6.** Current pulse waveforms for different damping coefficients.

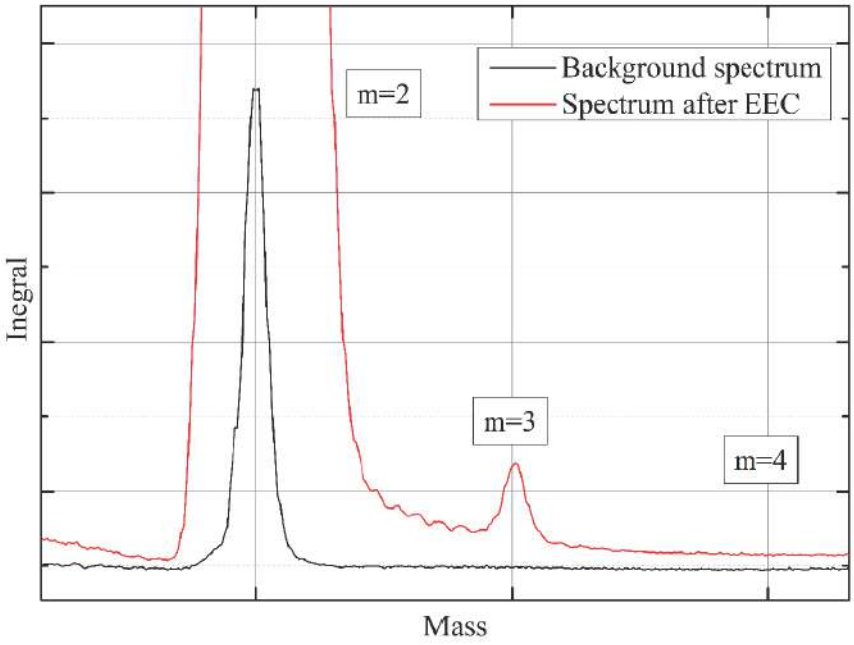


**Figure 7.** Mass spectrum fragment in the area of light masses.

number of $m = 4$ particles. Then, the valve connecting the explosion chamber with the leak detector was closed, and for several hours the pressure in the chamber grew, due to the diffusion of gas from chamber walls and leakage of air through the seals. Then the procedure of pumping gas through leak detector was repeated. The measurement results are shown on the graph (Fig. 9).

The figure shows that the rate of $m = 4$ particle formation after the electric explosion of tungsten wire decreases with time, and after the time $T \sim 70$ h it becomes constant. A possible explanation of the time dependence of the concentration of particles with $m = 4$ is that $^4$He atoms, formed during EEC, have high energy and are "hammered" into the surface of the quartz cylinder to a certain depth and then slowly diffuse out of the quartz chamber walls. It should be noted that helium has an abnormally high diffusion coefficient in quartz [26]. It can be seen from the curve form shown in Fig. 9 that after 70 h a leakage of helium from the atmosphere through the connecting seals becomes the primary mechanism which determines the formation of helium in the explosion chamber.

In order to ensure that the $m = 4$ particles detected after the electric explosion are indeed $^4$He atoms and their formation is due to the electric explosion of tungsten wire, a series of test experiments was carried out in which iron wire was used as a load. Iron wire was chosen because the $\alpha$-decay of iron isotopes is energetically forbidden, unlike tungsten isotopes. If the accumulation effect of $m = 4$ particles was associated only with external factors, then the time dependence of the particle accumulation rate after the electric explosion of iron wire would not have been different from the curve shown in Fig. 9. However, in experiments with iron, the wire leakage rate was constant and determined completely by the gas leakage from atmosphere. The number of $m = 4$ particles, measured within 2 h after the EEC of iron wire, was $(6.2 \pm 0.9) \times 10^{11}$ U/Pa, which corresponds to the natural concentration of helium in the atmosphere $(5.2 \pm 0.2) \times 10^{11}$ U/Pa. Whereas $m = 4$ particle concentration for the EEC of tungsten wire reached $6 \times 10^{12}$ U/Pa or higher. Thus, our verification experiments with iron wire allow us to reach a preliminary conclusion that a portion

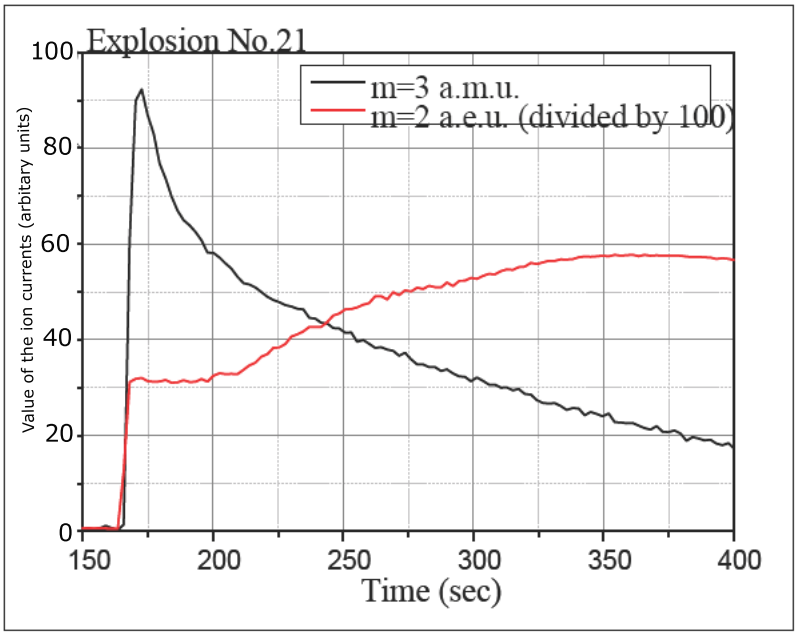


**Figure 8.** The time dependence of peaks $m = 2$ a.m.u. and $m = 3$ a.m.u.

of particles with $m = 4$ a.m.u. measured after EEC are connected with electric explosion of tungsten wire.

Attempts were made to establish the dependence of the measured amount of particles $m = 4$ with the length and diameter of the tungsten wire. However, because of the little excess of $m = 4$ particles over the background and lack of reproducibility of the experiments, statistically significant ($\sigma \geq 3$) results were not achieved.

### 3.3.2. *The results of measurements of optical methods*

The high sensitivity of the method, that combines prism optical monochromator UM-2 and image intensifier tube, allows us to obtain a panoramic spectrum of the visible range for each electric explosion of tungsten wire in vacuum.

Figure 10 shows the panoramic optical spectrum of light registered in the moment of electric explosion of tungsten wires of different diameters (10, 70 and 200 $\mu$m). The analyzed spectrum of optical radiation is located in the central area of each figure. The calibration spectra of mercury–helium and hydrogen lamps are located in the lower and upper areas. With its help the identification of the individual lines of the investigated range was made. The brightest lines in the examined spectrum were: H$\alpha$ line of atomic hydrogen ($\lambda_{\mathrm{H}\alpha} = 6563$ Å), and two lines in the red region, which could not be identified with the help of this diagnostic due to the low resolution of the UM-2 optical spectrometer.

As a rule, the panoramic spectrum was a combination of discrete and continuous spectra. However, continuum spectrum was practically absent (Fig. 10a) at small wire diameters (10 $\mu$m), and for large wire diameters (200 $\mu$m) the intensity of it was so great that in the red region of optical spectrum range a discrete component generally is not visible on the continuum spectrum background (Fig. 10c). As seen from Fig. 10b for the mid-value diameters (70 $\mu$m), the intensities of discrete and continuous spectrum were approximately the same.

The study of the behavior of time dependence of integral light intensity was carried out using a semiconductor

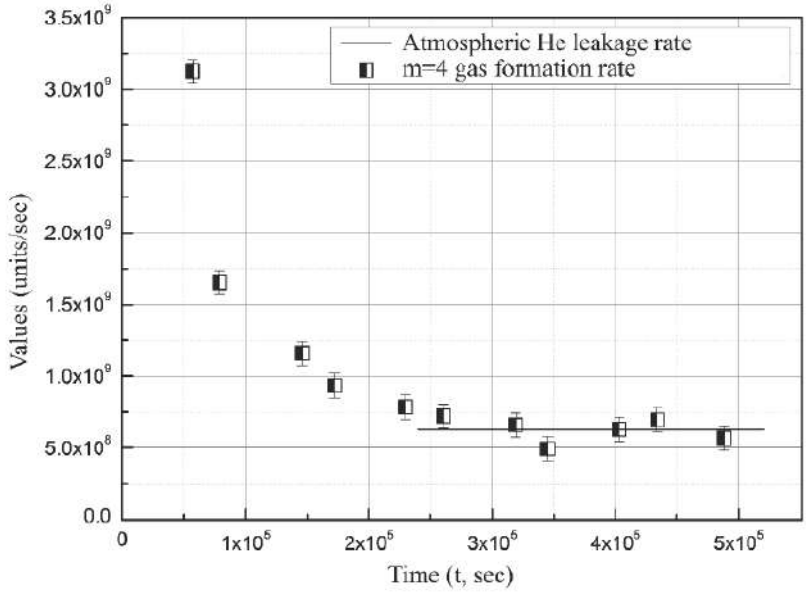


**Figure 9.** The rate of $m = 4$ particles formation in the chamber after the EEC (experiment No. 54).

photodiode in addition to the registration of the spectra. It has been found that for the wires with diameter larger than $100$ $\mu$m, radiation intensity has two maxima. The maximum intensity of the second peak occurs at approximately $200$ $\mu$s from the beginning of EEC. By this time, the capacitor bank has discharged almost completely, energy input into the wire has stopped, so the observed behavior of light seems very unexpected. The second peak does not appear for wires with a diameter of less than $100$ $\mu$m. The signals from the photodetector, adjusted to a common scale, are shown in Fig. 11.

Comparison of the spectral measurement results presented in Fig. 10 with the data from photodetector (Fig. 11) suggests that the presence of the first maximum of intensity of radiation is associated with a discrete component of the optical spectrum, and presence of a second peak – with a continuous component of the spectrum. This result is easily reproduced and was observed in each experiment with wires with diameters larger than $100$ $\mu$m. Based on the available experimental data, it is difficult to say anything certain about the physical cause of the second peak of integral light intensity. However, the fact that the distance between the light peaks does not depend of the diameter of exploded wire (see Fig. 11) suggests that the appearance of the second peak is associated with the plasma recombination on the chamber walls. Based on the above assumption, the average plasma expansion velocity can be estimated - $V_{\rm p} \sim 2\times 10^4 {\rm cm/s}$.

For a more precise identification of the spectral lines of optical radiation, an STE-1 spectrometer combined with the CCD array was used as a recording instrument. A few lines were observed in the panoramic spectra, but their identification was difficult due to the low resolution of the UM 2 spectrometer, so they were identified using the STE-1. They were: Na spectral lines double in the yellow region $\lambda_{\rm Na} = 5889$ to $5895$ Å (Fig. 12), atomic oxygen line $\lambda_{\rm O} = 7771\backslash 7774\backslash 7775$ Å (Fig. 13), and carbon ion line $\lambda_{\rm C+} = 7231$ to $7236$ Å (Fig. 14).

Comparing our results with the results of [1] we can assume that it was those lines that Wendt and Irion observed in their experiment, but were unable to decipher.

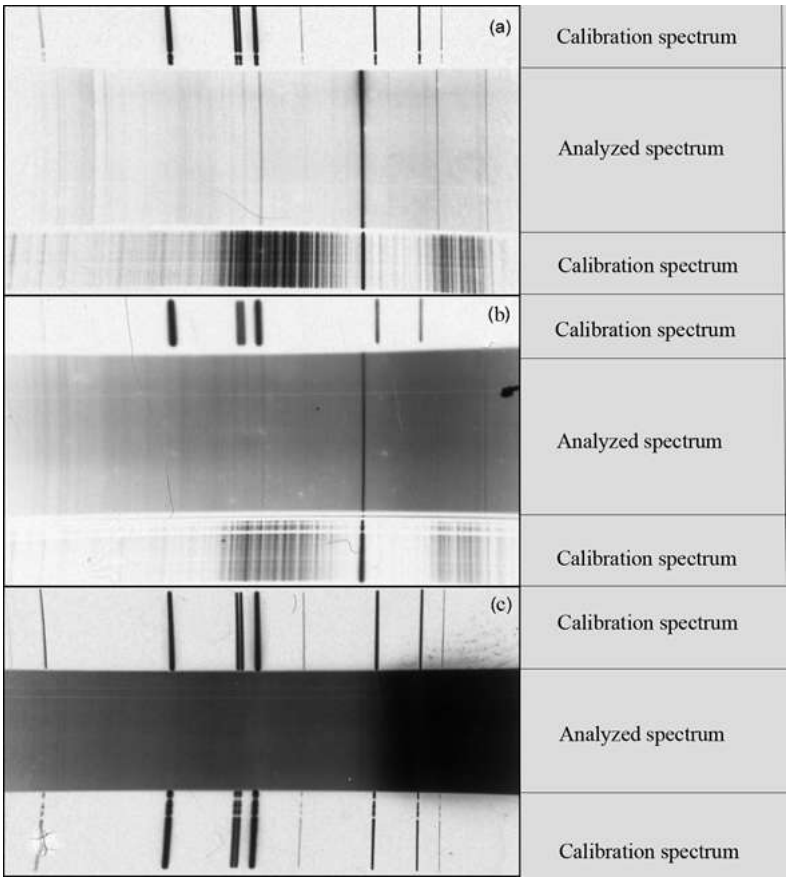


**Figure 10.** Panoramic radiation spectra of electric explosion of tungsten wires of different diameters: (a) 10 $\mu$m, (b) 70 $\mu$m and (c) 200 $\mu$m.

Registration of the emission spectrum of radiation with high resolution made it possible to measure the temperature of the electrons in the emerging tungsten plasma. A model of local thermodynamic equilibrium (LTE) has been used for the calculations [27,28]. Since the measurement of the absolute intensity of the lines – a very difficult task, the calculations use the relative intensities of the spectral lines, which were obtained through the study of individual spectral regions. Considering the possibility or strength of transition oscillator [29], tungsten plasma electron temperature has been determined for a number of spectral line pairs using the formula:

$$\frac{I_2}{I_1} = \frac{g_2}{g_1}\frac{f_2}{f_1}\frac{\lambda_1^3}{\lambda_2^3}\exp\left(-\frac{\Delta E}{kT_{\mathrm{e}}}\right),$$

where $I_{\mathrm{i}}$ is relative intensity of the tungsten spectral lines, $g_{\mathrm{i}}$ the statistical weight of levels, $f_{\mathrm{i}}$ the transition oscillator strength, $\lambda_{\mathrm{i}}$ the spectral line wavelength, $\Delta E$ the difference between the excitation energies of investigated lines and $T_{\mathrm{e}}$ is the plasma electron temperature. Table 2 shows the values required to calculate relative intensities of the tungsten lines, experimental and tabulated values are given in [29]:

Table 2 shows that the average electron temperature in the tungsten plasma, formed as a result of EEC, is about 0.5 eV. As it can be seen the plasma temperature was several times smaller than the value that Wendt and Irion were

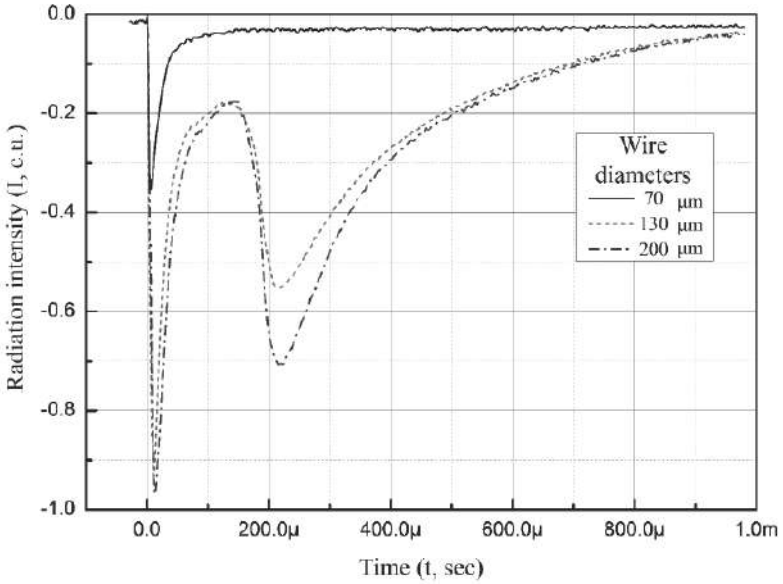


**Figure 11.** Time dependence of the integral light intensity for the wires of different diameters.

expected to reach in their experiments [1].

The data of optical spectral analysis and gas mass spectrometer showed clearly that the gas mixture with a high concentration of hydrogen appears in the explosion chamber after EEC. As for the helium presence in the gas phase formed after EEC, in many experiments, the data obtained with the help of the MS-40 indicated the presence of

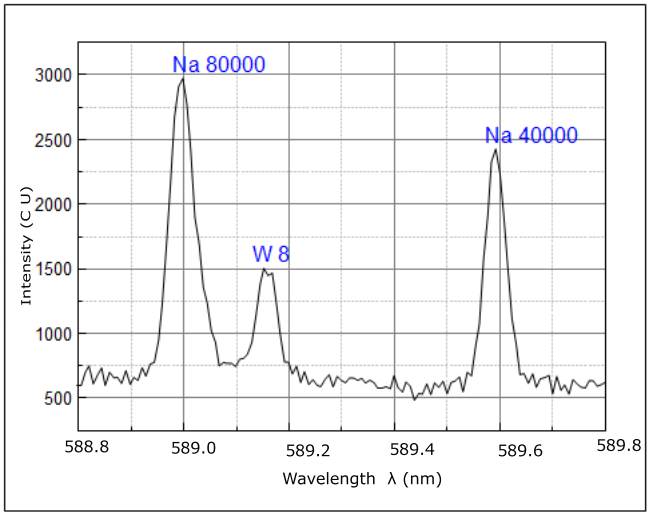


**Figure 12.** Fragment of high-resolution linear spectrum with Na spectral lines.

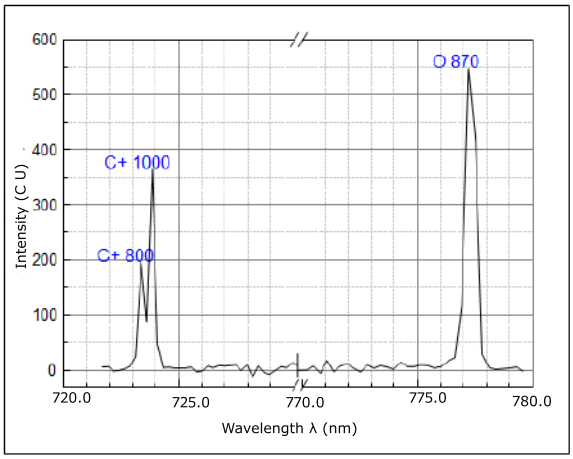


**Figure 13.** Fragment of spectrum with lines of atomic oxygen and carbon ion (next to the lines indicating its intensity, taken from a reference book) registered at the moment of the electric explosion using UM-2 with CCD-array as a recording element.

particles with $m = 4$ in the explosion chamber with a concentration greater than the concentration of $^4$He in the atmosphere, but the He optical lines were registered only in several experiments. Therefore, the influence of hydrogen on the emissivity of the helium atoms was studied. These studies were carried out in a hydrogen–helium medium at various ratios of the partial pressures of $^4$He and $H_2$.

The plasma discharge was excited in the explosion chamber using the capacitor bank of "HELIOS" setup. A test mixture with a known concentration $^4$He and $H_2$ was let into the chamber until the pressure is set up to $P \sim 1$ Torr, which is in order of magnitude corresponds to a pressure PB after the electric explosion. From verification experiments it follows that, with a ratio of $^4$He: $H_2 = 1:20$ the transition corresponding to $^4$He wavelength $\lambda_2 = 6678.15$ Å become barely visible, and strong molecular hydrogen line appears near the helium line with wavelength

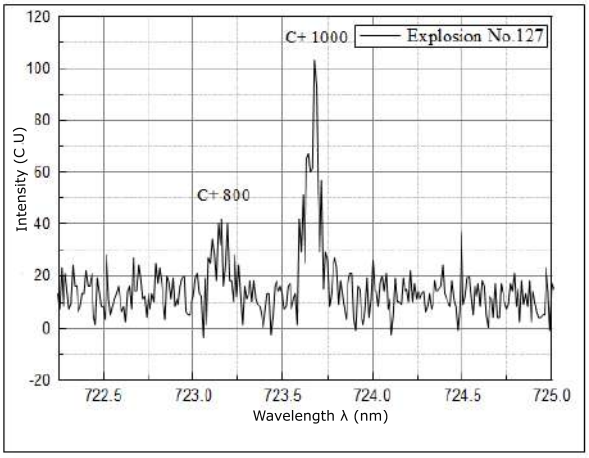


**Figure 14.** High resolution fragment of a spectrum with lines of carbon ion.

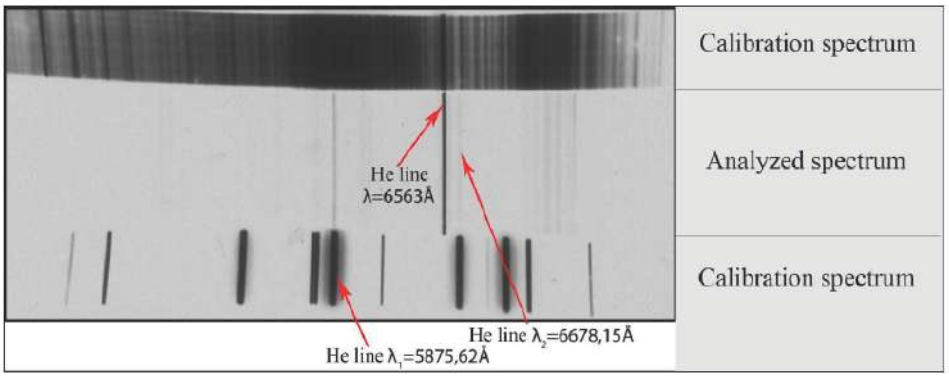


**Figure 15.** The radiation spectrum of gas mixture obtained after the series discharges.

$\lambda_1 = 5875.62$ Å. And with a ratio of $^4$He: $H_2 = 1 : 50$ helium line with a wavelength $\lambda_1 = 5875.62$ Å ceases to radiate at all. Apparently excitement is removed due to collisions with hydrogen molecules. From the conducted methodical work, it is clear that, without reducing the partial pressure of hydrogen in the resulting gas mixture, identification of helium by optical methods at the time of EEC seems unlikely.

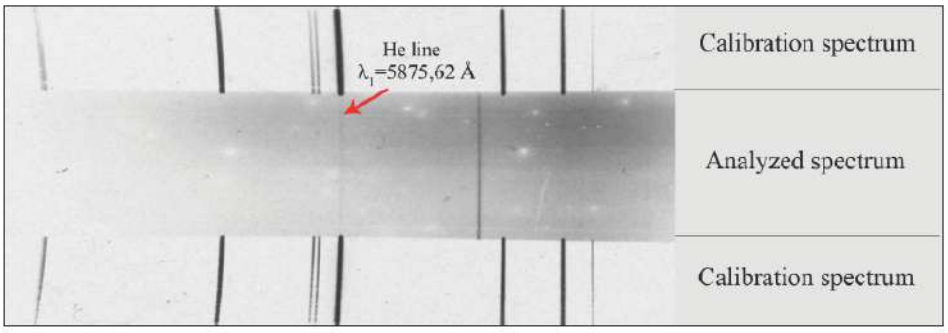


**Figure 16.** The radiation spectrum of the gas mixture obtained during the EEC.

**Table 2.** The values for the calculation of the electron plasma temperature.

| Λ(Å) | $I$(relative units) | $gf$, ea. | $E$(cm$^{-1}$) | $T_e$ (K) |
|---|---|---|---|---|
| 5864.63 | 800 | 0.036 | 36 874 | 4568 |
| 5804.87 | 1200 | 0.45 | 43 452 | |
| 5947.58 | 870 | 0.016 | 30 587 | 5295 |
| 5735.09 | 1000 | 0.82 | 44 920 | |
| 6964.12 | 130 | 0.0022 | 14 355 | 5893 |
| 7140.54 | 310 | 0.0046 | 14 000 | |

From the dependence shown in Fig. 9, it follows that the number of atoms with $m = 4$ a.e.u., measured using the helium leak detector within 1–3 h after the EEC, by an order of magnitude greater than when measured immediately after the EEC. It should be noted that this result was quite unexpected. In addition, almost all of the hydrogen formed in the explosion chamber as a result of the EEC is pumped out through the leak detector during the first measurement of particles and thereafter no longer found in the chamber. Consequently, in the gas phase formed after the first measurement, $^4$He:$H_2$ ratio is significantly higher than in the gas mixture formed immediately after the electric explosion. The latter circumstance allowed us to hope that in the gas mixture with a higher ratio of $^4$He:$H_2$ we will be able to detect the helium optical spectrum. For the implementation of this idea, the residual gas, which was formed within several hours after the EEC, was excited with the help of high-voltage pulses in a quartz chamber and, in these conditions the spectrum shown in Fig. 15 was detected.

Since during the aperiodic EEC regime hydrogen generation is less than during the EEC with high $Q$-value, the ratio of $^4$He:$H_2$ at the moment of electric explosion is higher. This fact led to the registration of $^4$He line ($\lambda_1 = 5875.62$ Å) directly at the moment of the EEC in one of the experiments. That spectrum is shown in Fig. 16.

#### 3.3.3. *The results of analysis of solid EEC product*

The analysis of surface of quartz fragments of the explosion chamber was carried out to determine the chemical composition of solid products of the tungsten wire explosion. The analysis of the inner surface of the quartz chamber, in which a series of EEC experiments with tungsten wires were made, was conducted using a scanning X-ray photoelectron microprobe (PHI Quantera SXM).

The X-ray fluorescence analysis showed the presence of carbon, sodium and nitrogen. The presence of nitrogen appears to indicate that the quartz, in the preparation stage of the experiment, was not heated properly, because this effect is usually observed as a result of quartz contact with air.

Typically, the presence of carbon and sodium is interpreted as surface contamination, but the outer side of the same quartz cylinder fragment did not show any traces of Na spectral lines. The presence of Na and C spectral lines on the inner surface of the quartz chamber fragment, identified using XPS, is consistent with the results obtained by means of optical methods. Therefore, the presence of these elements is apparently not due to contamination of its surface.

For mass spectrometric analysis of solid residues obtained as a result of EEC, a laser mass spectrometer with magnetic separation of ions was used, with sensitivity of $10^{-4}$–$10^{-5}$ at.%. Mass spectrometry analysis of the initial tungsten wire showed that it is made up of 98.5 at.% W atoms, and its original isotopic composition was totally natural. Isotopic analysis of the residues of tungsten wire after EEC showed a complete absence of tungsten isotope $^{180}$W, although in the initial wire, it was consistently detected at 0.14%. However, the statistical significance of these measurements is not sufficient to draw conclusions based on solid mass spectrometric measurements.

## 4. Conclusions

The following conclusions can be drawn from the data obtained.

(1) The amount of gas formed as a result of EEC of tungsten wire is $10^{18-19}$ atoms, which coincides with the data in [1]; but most of the gas is formed by desorption. We can assume that in [1], most of detected gas was also from impurities. There was no hydrogen in the explosion chamber, but mercury vapor (from the mercury pump) was present in the glass bulb used in [1], which greatly eased the excitement of the levels of helium atoms. Based on its parameters, the explosion chamber in [1] was identical to the mercury-helium lamp. Thus, the number of helium atoms formed during the electric explosion of tungsten wire [1] could be quite small
(2) Despite all measures taken we could not fully purge hydrogen from the system, which significantly complicated the diagnosis of He.

(3) In some experiments, the presence of particles with $m = 3$ a.m.u. was detected with confidence. It was not possible to identify it uniquely, but current article presents experimental arguments in favor of the hypothesis that the registered $m = 3$ particles could be $^3$He. This is an unexpected result, but it does not contradict the results of [1], although it is in contradiction with the stated theoretical premises.
(4) The presence of atoms with $m = 4$ a.m.u. was reliably detected in the gas mixture formed after the electric explosion, but on the basis of available data it is impossible to be sure that these are helium atoms. Quantitative measurements show that the concentration of $m$ = 4 atoms in the gas, formed after the electric explosion is higher than concentration of $^4$He atoms in air mixture.
(5) Contrary to expectations, the highest number of $m = 4$ atoms was detected not immediately after of EEC, but within 1–3 h after it.
(6) In results similar to [1], several bright lines in the red part of the optical spectrum were observed, which were identified with the help of modern techniques.
(7) No fast neutrons were observed during the EEC of tungsten wires.

Thus, the obtained results are not contrary to the results of Wendt and Irion. But, in order to confidently speak about presence of low energy nuclear reactions during EEC it is necessary to specify all the daughter nuclei and calculate the energy balance of reactions.

## Acknowledgements

To our great regret, due to circumstances beyond our control, the present study remains unfinished, but it is still a pleasant duty to thank our colleagues for their help in carrying out the experiments: V.I. Mizhiritskii and R.M. Arshba, as well as our younger colleagues, students of MIPT: P.V. Belous, T.V. Shpakovskii, G.K. Steshenko, G.I. Zhotikov, A.A. Levanov and A.V. Steblevskii (IGIC RAS) for carrying out a solid mass spectrometry analysis; I.L. Fedechkin (Ioffe Institute) for help with the gas mass spectrometry; E.G. Silkisu (Institute for Spectroscopy RAS) for help with the optical spectroscopy; D.V. Petrov (Skobeltsyn Institute of Nuclear Physics MSU) for carrying out analyzes on a scanning microscope; B.A. Lazba (Sukhumi Institute of Physics and Technology) for organizational support in the establishment of the laboratory and during the experiments. Special gratitude is for Anri Amvrosievich Rukhadze for interest in the work, stimulating discussions and scientific support.

## References

[1] G. L. Wendt and C.E. Irion, Experimental attempts to decompose tungsten at high temperatures, *Amer. Chem. Soc*., Chicago **44** (1922) 1887–1894, Contribution from the Kent Chemical Laboratory, University of Chicago.
[2] J.A. Anderson, The spectrum of electrically exploded wires, *Astrophys. J*. **51,** pp. 37–48.
[3] E. Rutherford, *Nature* London **109** (1922) 418.
[4] G.L. Wendt, *Science* **55** (1922) 567.
[5] A.A. Volkov, A.P. Govorun, A.A. Gulyaev et al., Study of electric explosion of wires with microsecond current pulses in a longitudinal magnetic field (in Russian), *Zhurnal-tekhnicheskoj fiziki* **72** (2002) 115–120.
[6] A.A. Rukhadze (Ed.), Exploding wires (in Russian), Moscow, IL, 1963.
[7] A.A. Rukhadze and I.S. Shpigel (Eds.), *Electrical Explosion of Conductors* (in Russian), Moscow, MIR, 1965.
[8] A.G. Russkih, R.B. Baksht, A. Yu. Labetsky et al., Influence of polarity of the high voltage electrode and pre-heating of tungsten micro-strip on its power characteristics in an explosion in vacuum (in Russian), *Fizika Plasmi*. Moscow **32**(10) (2006) 893–906.
[9] V.A. Gribkov, Encyclopedia of low-temperature plasma (in Russian), Moscow: Yanus K **IX-3** (2007) 288–332.
[10] S.S. Ananiev, Y.L. Bakshaev, P.I. Blinov et al. (in Russian), *Fizika Plasmi*. **36**(6) (2010) 1–9.
[11] G.S. Volkov E.V. Grabowski, K.N. Mitrofanov and G.M. Oleinik (in Russian), *Fizika Plasmi*. **30** (2) (2004) 99.

[12] R.B. Spielman, C. Deeney, G.A. Chandler et al., *Phys. of Plasmas* **5**(5) (1998) 2105–2112.
[13] C. Cozzini et al., *Phys. Rev.* C **70** (2004) 064606.
[14] O. Bohr and B. Mottelson, *Nuclear Structure*, Vol. 1, Benjamin, New York, Amsterdam, 1969.
[15] V.A. Erma, *Phys. Rev*. **105** (1957) 1784.
[16] D.V. Filippov, A.A. Rukhadze and L.I. Urutskoev, *Ann. Fond. L.de Broglie* **29** Hors Serie No. 3 (2004) 1207–1217.
[17] S.V. Starodubtsev and A.M. Romanov, Radioactive transformations nuclei and nuclear envelope (in Russian), Tashkent: Publising House, *Proc. Akad. Uzbek SSR*, 1958, p. 495.
[18] L.I. Urutskoev and D.V. Filippov, *Physics-Uspekhi*. **47**(12) (2004) 1257–1260.
[19] H. Hatting, K. Hunchen and H. Waffer, *Phys. Rev. Lett.* **25** (1970) 941.
[20] D.V. Filippov, L.I. Urutskoev, A.O. Biryukov, A.A. Rukhadze and P.V. Bilous (in Russian), *Prikladnaya Fizika* **4** (2012) 5–14.
[21] F. Bosch, T. Faestermann, J. Friese et al., *Phys. Rev. Lett.* **77**(26) (1996) 5190–5193.
[22] D.V. Filippov, *Phys. Atomic Nuclei* **70** (2) (2007) 258–264; **70**(12) (2007) 2016–2024.
[23] L.I. Urutskoev, A.A. Rukhadze, Filippov D.V. et al., Study of the spectral composition of optical radiation during electrical explosion of a tungsten wire, *Bulletin Lebedev Phys. Institute* **39**(7) (2012) 199–203.
[24] N.N. Aruev, A.V. Kozlovsky, I.L. Fedichkin et al. (in Russian), *JTP Lett.* **23** (1997) 83, 87.
[25] Akulov, Yu. A. et al., Helium-isotope mass-spectrometric method for studying tritium beta decay (idea, experiment, nuclear and molecular physics applications), *Physics-Uspekhi* **46**(11) (2003) 1153.
[26] J. Groszkowski, Technika wyskiej prozni, Wydawnictwa Naukowo-Technczne, Warszawa, 1972.
[27] R. Haddltstoun and S. Leonard, *Plasma Diagnostics* (in Russian), S. Yu. Lukyanova (Ed.), MIR, Moscow, 1967, 165 p.
[28] Collection of Reports: Temperature and Its Measurement (in Russian), A. Armand and K. Wolfson, Moscow, Publishing House of Foreign Literature, 1960.
[29] C. Corliss and W. Bozeman, The Transition Probabilities and Oscillator Strength Of 70 Elements (in Russian), R. Zolina (Ed.), MIR, Moscow, 1968, 515–518.